

RIGOROUS STABILITY RESULTS FOR A LAPLACIAN MOVING BOUNDARY PROBLEM WITH KINETIC UNDERCOOLING*

UTE EBERT , BERNARD MEULENBROEK[†], AND LOTHAR SCHÄFER[‡]

Abstract. We study the shape stability of disks moving in an external Laplacian field in two dimensions. The problem is motivated by the motion of ionization fronts in streamer-type electric breakdown. It is mathematically equivalent to the motion of a small bubble in a Hele-Shaw cell with a regularization of kinetic undercooling type, namely a mixed Dirichlet-Neumann boundary condition for the Laplacian field on the moving boundary. Using conformal mapping techniques, linear stability analysis of the uniformly translating disk is recast into a single PDE which is exactly solvable for certain values of the regularization parameter. We concentrate on the physically most interesting exactly solvable and non-trivial case. We show that the circular solutions are linearly stable against smooth initial perturbations. In the transformation of the PDE to its normal hyperbolic form, a semigroup of automorphisms of the unit disk plays a central role. It mediates the convection of perturbations to the back of the circle where they decay. Exponential convergence to the unperturbed circle occurs along a unique slow manifold as time $t \rightarrow \infty$. Smooth temporal eigenfunctions cannot be constructed, but excluding the far back part of the circle, a discrete set of eigenfunctions does span the function space of perturbations. We believe that the observed behaviour of a convectively stabilized circle for a certain value of the regularization parameter is generic for other shapes and parameter values. Our analytical results are illustrated by figures of some typical solutions.

Key words. moving boundaries, kinetic undercooling, Laplacian growth, streamer discharges, convective stabilization

AMS subject classifications. 37L15, 37L25, 76D27, 80A22, 78A20

1. Introduction.

1.1. Problem formulation in physical and mathematical context. The mathematical model considered in this paper is motivated by the physics of electric breakdown of simple gases like nitrogen or argon [1, 2, 3, 4, 5]. During the initial ‘streamer’ phase of spark formation, a weakly ionized region extends in a strong externally applied electric field. As the ionized cloud is electrically conducting, it screens the electric field from its interior by forming a thin surface charge layer. This charged layer moves by electron drift within the local electric field and creates additional ionization, i.e., additional electron–ion–pairs, by collisions of fast electrons with neutral molecules. We here approximate the ionized and hence conducting bulk of the streamer as equipotential. In the non-ionized and hence electrically neutral region outside the streamer, the electric field obeys the Laplace equation. The thin surface charge layer can be approximated as an interface which moves according to the electric field extrapolated from the neutral region onto the interface. We therefore are concerned with a typical moving boundary problem.

Such moving boundary problems occur in various branches of physics, chemistry or biology. The most extensively studied examples are viscous fingering observed in two-fluid flows [6] or the Stefan problem of solidification from an undercooled melt [7]. Other physical phenomena like the motion of voids in current carrying metal films [8] lead to similar mathematical models [9].

We here discuss the streamer model in two spatial dimensions, where in the simplest ‘unregularized’ version the basic equations coincide with those describing the

*The work of B.M. was supported by a Ph.D. position from CWI Amsterdam.

[†]U.E. and B.M. work at CWI, P.O.Box 94079, 1090GB Amsterdam, The Netherlands. U.E. also holds a parttime appointment at Eindhoven Univ. Techn., The Netherlands.

[‡]L.S. works at Universität Duisburg–Essen, Universitätsstr. 5, 45117 Essen, Germany.

motion of a small bubble in a liquid streaming through a Hele-Shaw cell [10, 11, 12, 13], which is a special case of two fluid flow. The unregularized streamer model has been discussed in Ref. [4, 14]. Restriction to two dimensions in space allows us to use standard conformal mapping techniques [6, 15] to reduce the moving boundary problem to the analysis of the time dependence of the conformal map that maps the unit disk to the exterior of the streamer.

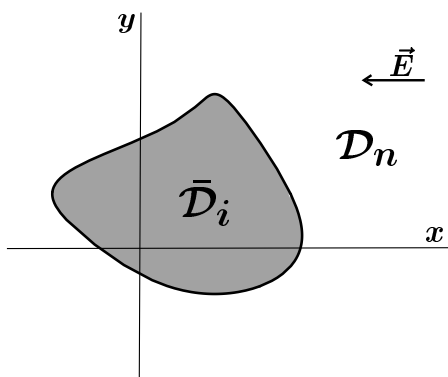
It is well known that unregularized moving boundary problems of this type are mathematically ill posed [15], in the sense that the moving interface generically develops cusps within finite time which leads to a breakdown of the model. To suppress such unphysical behavior, the models are regularized by imposing nontrivial boundary conditions on the interface. For viscous fingering typically some curvature correction to the interfacial energy is considered. For the streamer problem a mixed Dirichlet-Neumann boundary condition can be derived [14, 16] by analyzing the variation of the electric potential across the screening layer. Such a boundary condition is well known from the Stefan problem, where it is termed ‘kinetic undercooling’. It rarely has been considered for Hele-Shaw type problems. There are strong hints [15, 17, 18, 19] but no clear proof that it suppresses cusp formation.

1.2. Overview over main results and structure of the paper. Regularization of the streamer model introduces some parameter ϵ that measures the effective width of the interface relative to the typical size of the ionized region. The regularized problem allows for a class of solutions of the form of uniformly translating circles, and linear stability analysis of these solutions can be reduced to solving a single partial differential equation. For the special case $\epsilon = 1$, the general solution of this PDE can be found analytically, as we discussed in [14].

In the present paper we discuss the special case $\epsilon = 1$ in much more detail since the results show interesting and probably generic features. In particular, we find that the dynamics of infinitesimal perturbations are governed by a subgroup of the automorphisms of the unit disk. Generically, these automorphisms convect the perturbations to the back of the moving body. Initially, perturbations might grow, but asymptotically for time $t \rightarrow \infty$, they decay exponentially. Furthermore, this final convergence back to the unperturbed circle follows some universal slow manifold. Also a finite perturbation evolving under the linearized dynamics shows this behaviour, provided the initial perturbation obeys some simple bound. The subgroup of automorphisms leading to convective stabilization also governs the dynamics in another exactly solvable case: $\epsilon = \infty$, and since it for all $\epsilon > 0$ is intimately related to the characteristic curves of the PDE, we expect convective stabilization to hold generally for $\epsilon > 0$.

Analyzing the time evolution determined by a PDE, one often searches for eigenfunctions showing purely exponential time behaviour. For the present problem in a space of functions representing smooth initial perturbations of the moving circle, no such eigenfunctions exist. They can only be constructed if we allow for singularities on the boundary. Nevertheless a subset of these functions with time dependence $e^{-n\tau}$, $n \in \mathbf{N}_0$, is intimately related to the asymptotic convergence of the perturbations. Furthermore, in some restricted sense, it forms a complete set in function space.

This paper is organized as follows. In Sect. 2 we introduce the model, and the linear stability analysis of translating circles is carried through in Sect. 3. These two sections are extended versions of Ref. [14], where also a short account of results for the case of $\epsilon = 1$ has been presented. The detailed discussion of this case of strong screening is the topic of this paper. Analytical results based on the PDE of linear

FIG. 2.1. Geometry of the streamer model, \vec{E} is the constant far field.

stability analysis are derived in Sect. 4, and explicit examples are presented in Sect. 5. Sect. 6 summarizes our conclusions. The appendix contains a discussion of another rigorously solvable case, namely $\epsilon = \infty$.

We finally should note that in a true electrical discharge the typical streamer is an elongated object frequently connected to an electrode, rather than an uniformly translating closed body. Thus the uniformly translating circles, which form the basis of our analysis, are somewhat unphysical, in particular with respect to the physics at their backside. We nevertheless for shortness will address these solutions as ‘streamer’, being well aware that this is a slight abuse of this term.

2. Physical model and conformal mapping approach.

2.1. The model. We assume the ionized bulk of the streamer to be a compact, simply connected domain $\bar{\mathcal{D}}_i$ of the (x, y) -plane. Outside the streamer, i.e. in the open domain \mathcal{D}_n , there are no charges and the electric potential obeys the Laplace equation

$$(2.1) \quad \Delta\varphi = 0 \quad \text{for } (x, y) \in \mathcal{D}_n.$$

The streamer moves in an external electric field that becomes homogeneous far from the ionized body; therefore the electric potential φ at infinity obeys the boundary condition

$$(2.2) \quad \varphi \rightarrow E_0 x + \text{const} \quad \text{for } \sqrt{x^2 + y^2} \rightarrow \infty.$$

This equation excludes a contribution to φ diverging as $\ln(x^2 + y^2)$ which implies that the total charge due to electrons and ions vanishes within $\bar{\mathcal{D}}_i$ and that the far field has the form

$$\vec{E} = -\nabla\varphi \rightarrow -E_0 \hat{\mathbf{x}},$$

where $\hat{\mathbf{x}}$ is the unit vector in x -direction. On the surface of the streamer we impose the boundary condition

$$(2.3) \quad \varphi = \ell \hat{\mathbf{n}} \cdot \nabla\varphi,$$

where $\hat{\mathbf{n}}$ is the unit vector normal to the surface pointing into \mathcal{D}_n . Here as well in Eq. (2.4) below it is understood that the surface is approached from \mathcal{D}_n . As mentioned

in the introduction, this boundary condition results from the analysis of the variation of the potential across the interface, and the length parameter ℓ can be interpreted as the effective thickness of the screening layer. The case $\ell = 0$ corresponds to the unregularized case with a pure Dirichlet condition on the moving boundary. Dynamics is introduced via the relation

$$(2.4) \quad v_n = \hat{n} \cdot \nabla \varphi,$$

which holds on the boundary and determines its normal velocity v_n . This defines our model. For further discussion of its physical background, we refer to [1, 2, 3, 4, 5].

Now obviously, E_0 can be absorbed into a rescaling of the potential φ and of the time scale inherent in the velocity v_n , therefore henceforth we take $E_0 = 1$. Clearly the model defined here is most similar to a model of the motion of a small bubble in a Hele-Shaw cell [11, 12], except that the boundary condition (2.3) is of the form of a kinetic undercooling condition [17, 18].

2.2. Conformal mapping. A standard approach to such moving boundary problems proceeds by conformal mapping [6, 14]. We identify the (x, y) -plane with the closed complex plane $z = x + iy$, and we define a conformal map $f(\omega, t)$ that maps the unit disk \mathcal{U}_ω in the ω -plane to \mathcal{D}_n in the z -plane, with $\omega = 0$ being mapped on $z = \infty$

$$(2.5) \quad z = f(\omega, t) = \frac{a_{-1}(t)}{\omega} + \hat{f}(\omega, t), \quad a_{-1}(t) > 0.$$

By virtue of Eq. (2.1), the potential φ restricted to \mathcal{D}_n is a harmonic function, therefore it is the real part of some analytic function $\tilde{\Phi}(z)$, which under the conformal map (2.5) transforms into

$$(2.6) \quad \Phi(\omega, t) = \tilde{\Phi}(f(\omega, t)) = \frac{a_{-1}(t)}{\omega} + \hat{\Phi}(\omega, t).$$

The pole results from the boundary condition (2.2) with $E_0 = 1$. The functions \hat{f} and $\hat{\Phi}$ are holomorphic for $\omega \in \mathcal{U}_\omega$, and we assume that the derivatives ∂_ω^n of all orders n exist on the unit circle $\partial\mathcal{U}_\omega$. This restricts our analysis to smooth boundaries of the streamer. (Weaker assumptions on boundary behavior briefly will be discussed in Sect. 4.8.) Conditions (2.3) and (2.4) take the form

$$(2.7) \quad |\omega \partial_\omega f| \Re[\Phi] = -\ell \Re[\omega \partial_\omega \Phi] \quad \text{for } \omega \in \partial\mathcal{U}_\omega,$$

$$(2.8) \quad \Re \left[\frac{\partial_t f}{\omega \partial_\omega f} \right] = \frac{\Re[\omega \partial_\omega \Phi]}{|\omega \partial_\omega f|^2} \quad \text{for } \omega \in \partial\mathcal{U}_\omega.$$

Eqs. (2.5) – (2.8) form the starting point of our analysis.

3. Linear stability analysis of translating circles.

3.1. Uniformly translating circles. A simple solution of Eqs. (2.7), (2.8) takes the form

$$(3.1) \quad \begin{cases} f^{(0)}(\omega, t) &= \frac{R}{\omega} + \frac{2R}{R+\ell} t, \\ \Phi^{(0)}(\omega, t) &= R \left[\frac{1}{\omega} - \frac{R-\ell}{R+\ell} \omega \right]. \end{cases}$$

In physical coordinates x and y , it describes circles of radius $R > 0$ centered at $x(t) = v_0 t$ and moving with velocity $v_0 = 2R/(R+\ell)$ in direction $\hat{\mathbf{x}}$. Thus the point $\omega = 1$ maps to a point at the front and the point $\omega = -1$ maps to a point at the back of the streamer. These points will play a crucial role in our analysis.

We note that the one-parameter family (3.1) of solutions parametrized by R , that is found in the regularized model, is a subset of the two-parameter family found in the unregularized case $\ell = 0$. As is well known, for $\ell = 0$ all ellipses with one axis parallel to $\hat{\mathbf{x}}$ are uniformly translating solutions [10].

3.2. Derivation of the operator \mathcal{L}_ϵ for linear stability analysis. We now derive the equation governing the evolution of infinitesimal perturbations of the circles (3.1). In general, the parameter R can become time dependent. We use the ansatz

$$(3.2) \quad \begin{cases} f(\omega, t) &= \frac{R(t)}{\omega} + x(t) + \eta \beta(\omega, t), \\ \Phi(\omega, t) &= R(t) \left[\frac{1}{\omega} - \frac{R(t)-\ell}{R(t)+\ell} \omega + \eta \chi(\omega, t) \right], \\ \partial_t x(t) &= \frac{2R(t)}{R(t)+\ell}, \quad R(t) > 0, \end{cases}$$

where η is a small parameter. However, working to first order in η it is found that R stays constant. This results from the fact that the dynamics embodied in Eq. (2.8) strictly conserves the area $|\bar{\mathcal{D}}_i|$ of the streamer, which in this context is the equivalent to the temporal conservation of the zero order Richardson moment [13, 15, 20], but integrated over the complement of \mathcal{D}_n . In terms of the mapping f , the conserved area $|\bar{\mathcal{D}}_i|$ can be written as

$$(3.3) \quad \begin{aligned} |\bar{\mathcal{D}}_i| &= \left| \int_0^{2\pi} d\alpha \left(\Re [f(e^{i\alpha}, t)] - x(t) \right) \partial_\alpha \Im [f(e^{i\alpha}, t)] \right| \\ &= \pi R^2(t) - \eta^2 \int_0^{2\pi} d\alpha \Re [\beta(e^{i\alpha}, t)] \partial_\alpha \Im [\beta(e^{i\alpha}, t)]. \end{aligned}$$

Now introducing the time independent length R_0 through $|\bar{\mathcal{D}}_i| = \pi R_0^2$, we find $R(t) = R_0 + \mathcal{O}(\eta^2)$, which proves that R is time independent within linear perturbation theory. In the sequel we will use R_0 as our length scale, introducing

$$(3.4) \quad \epsilon = \frac{\ell}{R_0} \quad \text{and} \quad \tau = \frac{2}{1+\epsilon} \frac{t}{R_0},$$

and rescaling f and Φ by factors $1/R_0$. We note that within the dimensionless time intervall $\Delta\tau = 1$, the streamer moves a distance of the order of its size.

With the thus simplified ansatz (3.2), Eqs. (2.7) and (2.8) evaluated to first order in η take the form

$$(3.5) \quad \begin{cases} \Re \left[\omega(\partial_\omega - \partial_\tau)\beta - \frac{1+\epsilon}{2}\omega\partial_\omega\chi \right] = 0, \\ \Re \left[\epsilon(\omega^2 + 1)\omega\partial_\omega\beta - (1+\epsilon)(1 + \epsilon\omega\partial_\omega)\chi \right] = 0, \end{cases} \quad \text{for } \omega \in \partial\mathcal{U}_\omega.$$

Since β and χ are holomorphic for $\omega \in \mathcal{U}_\omega$, these equations imply

$$(3.6) \quad \begin{cases} \omega(\partial_\omega - \partial_\tau)\beta - \frac{1+\epsilon}{2}\omega\partial_\omega\chi = 0, \\ \epsilon(\omega^2 + 1)\omega\partial_\omega\beta - (1+\epsilon)(1 + \epsilon\omega\partial_\omega)\chi = ia, \end{cases} \quad \text{for } \omega \in \mathcal{U}_\omega,$$

where a is some real constant. Elimination of χ yields

$$(3.7) \quad \mathcal{L}_\epsilon\beta = 0,$$

where \mathcal{L}_ϵ is the operator

$$(3.8) \quad \mathcal{L}_\epsilon = \frac{\epsilon}{2} \partial_\omega (\omega^2 - 1)\omega \partial_\omega + \epsilon \omega \partial_\omega \partial_\tau + (1 + \epsilon) \partial_\tau - \partial_\omega.$$

3.3. Normal form of \mathcal{L}_ϵ and induced automorphisms of the unit disk. It is instructive to transform \mathcal{L}_ϵ to the normal form of a hyperbolic differential operator. We introduce

$$(3.9) \quad T = \tanh \frac{\tau}{2},$$

mapping the time interval $\tau \in [0, \infty[$ to $T \in [0, 1[$, and

$$(3.10) \quad \zeta = \frac{\omega + T}{1 + \omega T},$$

to find

$$(3.11) \quad \mathcal{L}_\epsilon = \epsilon h(\zeta, T) \partial_T \partial_\zeta + \frac{\partial h(\zeta, T)}{\partial T} \partial_\zeta + (1 + \epsilon) \partial_T,$$

$$(3.12) \quad h(\zeta, T) = \frac{\omega}{\partial_\zeta \omega} = \frac{(\zeta - T)(1 - T\zeta)}{1 - T^2}.$$

This identifies the manifolds $T = \text{const}$ or $\zeta = \text{const}$ as the characteristic manifolds of our problem for all $\epsilon \neq 0$.

As function of the ‘time-like’ parameter T , $0 \leq T < 1$, the transformation $\zeta = \zeta(\omega, T)$ in Eq. (3.10) represents a semigroup of automorphisms of the unit disk, with fixed points

$$\zeta = \omega = \pm 1.$$

For $T \rightarrow 1$, corresponding to $\tau \rightarrow \infty$, all points $\omega \neq -1$ are mapped into $\zeta = +1$, so that the large time behavior of any perturbation is governed by this attractive fixed point.

3.4. Analytical solutions of Eq. (3.7) for special values of ϵ . The general solution of Eq. (3.7) can be found analytically for the special values $\epsilon = 0$, $\epsilon = \pm 1$ and $\epsilon = \infty$. In the unregularized case $\epsilon = 0$, evidently any function

$$\beta(\omega, \tau) = \tilde{\beta}(\omega + \tau)$$

is a solution, and any singularity of $\tilde{\beta}$ found in the strip

$$0 < \Re[\omega] < \infty, \quad -1 \leq \Im[\omega] \leq 1$$

will lead to a breakdown of perturbation theory within finite time. This is the fingerprint of the ill-posedness of the problem for $\epsilon = 0$.

For $\epsilon = -1$, $\beta(\omega, \tau)$ generically for all $\tau > 0$ has a logarithmic singularity at $\omega = -T(\tau)$. We recall that negative values of $\epsilon = \ell/R_0$ imply negative thickness of the screening layer and thus are of no physical interest.

The case $\epsilon = +1$ is discussed in detail in the remainder of the paper. Though a regularization length ℓ identical to the object size R_0 is somewhat artificial, it is accessible to rigorous analytical treatment and we expect it to reveal generic features of the behavior for $\epsilon > 0$.

This is supported by the results for $\epsilon = \infty$ which show essentially the same features as the results for $\epsilon = 1$ below. Though the limit $\epsilon \rightarrow \infty$ is physically absurd when applied to streamers, it is worth studying with respect to the properties of the operator \mathcal{L}_ϵ , and we present a short discussion in the appendix.

4. Strong screening: analytical results for $\epsilon = 1$.

4.1. Analytical solution of the general initial value problem. With the form (3.11) of \mathcal{L}_ϵ , the PDE (3.7) for $\epsilon = 1$ reduces to

$$(4.1) \quad \partial_T \left(2 + h(\zeta, T) \partial_\zeta \right) \beta = 0,$$

showing that the function

$$(4.2) \quad G(\zeta) = (2 + h(\zeta, T) \partial_\zeta) \beta$$

is independent of T . To determine β , we use Eq. (3.12): $h(\zeta, T) = \omega / \partial_\zeta \omega$ to find

$$(4.3) \quad (2 + \omega \partial_\omega) \beta(\omega, \tau) = G(\zeta), \quad \zeta = \zeta(\omega, T(\tau)).$$

The solution regular at $\omega = 0$ takes the form

$$(4.4) \quad \beta(\omega, \tau) = \int_0^\omega \frac{x dx}{\omega^2} G \left(\frac{x + T(\tau)}{1 + xT(\tau)} \right).$$

A second independent solution is singular in $\omega = 0$:

$$(4.5) \quad \beta_{\text{sing}}(\omega, \tau) \equiv \frac{1}{\omega^2}.$$

The function G in the regular solution (4.4) is determined by the initial condition $\beta(\omega, 0)$ through

$$(4.6) \quad G(\omega) = (2 + \omega \partial_\omega) \beta(\omega, 0).$$

It thus is holomorphic for ω in the unit disk \mathcal{U}_ω and all derivatives exist on $\partial \mathcal{U}_\omega$, since we assume the initial surface to be smooth. Eq. (4.4) then shows that $\beta(\omega, \tau)$ inherits these properties for all $\tau < \infty$.

4.2. Automorphism of unit disk and a bound on the perturbation. It is now clear that the automorphisms $\zeta(\omega, T)$ of \mathcal{U}_ω from Eq. (3.12) contain the basic dynamics and, as shown in the appendix, this also holds for $\epsilon = \infty$. This is to be contrasted to the unregularized case $\epsilon = 0$, where the dynamics amounts to a translation of the unit disk. With the present dynamics, in the course of time larger and larger parts $\mathcal{U}(\delta)$ of the unit disk \mathcal{U}_ω are mapped to an arbitrarily small neighbourhood $|\zeta - 1| < \delta$ of the attractive fixed point $\zeta = 1$. According to Eqs. (4.4) and (4.6), the initial condition in the neighbourhood $|\omega - 1| < \delta$ then determines the evolution of $\beta(\omega, \tau)$ in all $\mathcal{U}(\delta)$. As a consequence, any pronounced structure found initially near ω_0 , $|\omega_0 - 1| > \delta$, is convected towards $\omega = -1$. Quantitatively this behavior is embodied in Eq. (4.17) below, and explicit examples will be presented in section 5, see, in particular, figure 5.4b.

For the further discussion we normalize $G(\omega)$ so that

$$(4.7) \quad \max_{|\omega|=1} G(\omega) = 1.$$

Eqs. (4.4), (4.7) yield a bound on $\beta(\omega, \tau)$:

$$(4.8) \quad |\beta(\omega, \tau)| \leq \frac{1}{2}; \quad |\omega| \leq 1, \quad 0 \leq T \leq 1.$$

Thus the perturbation can shift the position of the streamer at most by $\eta/2$, and therefore it cannot affect the asymptotic velocity of the propagation.

4.3. Center of mass motion for $0 \leq \tau < \infty$. In precise terms the position of the streamer can be defined as the center of mass

$$(4.9) \quad z_{\text{cm}} = x_{\text{cm}} + iy_{\text{cm}} = \frac{1}{|\mathcal{D}_i|} \int_{\mathcal{D}_i} dx dy (x + iy),$$

where the integral is related to the first order Richardson moment. Evaluating Eqs. (4.9) and (4.4), we find to first order in η

$$(4.10) \quad z_{\text{cm}} = \tau + \eta \beta(0, \tau),$$

$$(4.11) \quad \beta(0, \tau) = \frac{G(T(\tau))}{2}.$$

Here τ is the uniform translation of the unperturbed circle. The additional center of mass motion (4.11) for all times is explicitly given by the initial condition $\beta(\omega, 0)$ through Eq. (4.6) and the transformed time variable $T(\tau)$ from Eq. (3.9); for $\tau \rightarrow \infty$, it approaches $\beta(0, \tau) \rightarrow G(1)/2$.

4.4. Internal motion: convergence along a universal slow manifold for $\tau \rightarrow \infty$. We now concentrate on the perturbation of the circular shape, given by

$$(4.12) \quad \tilde{\beta}(\omega, \tau) = \beta(\omega, \tau) - \beta(0, \tau).$$

The explicit expression

$$(4.13) \quad \tilde{\beta}(\omega, \tau) = \int_0^1 d\rho \rho \left[G\left(\frac{\rho\omega + T}{1 + \rho\omega T}\right) - G(T) \right]$$

yields

$$(4.14) \quad \lim_{\tau \rightarrow \infty} \tilde{\beta}(\omega, \tau) = 0$$

for arbitrary G , i.e. for arbitrary initial condition (4.6). Thus the shape perturbation converges to zero as $\tau \rightarrow \infty$, and the circular shape is linearly stable.

We note that this holds despite the fact that the limits $\omega \rightarrow -1$ and $\tau \rightarrow \infty$, (i.e. $T \rightarrow 1$), do not commute

$$\begin{aligned} \lim_{T \rightarrow 1} \lim_{\omega \rightarrow -1} G(\zeta(\omega, T)) &= G(-1), \\ \lim_{\omega \rightarrow -1} \lim_{T \rightarrow 1} G(\zeta(\omega, T)) &= G(+1). \end{aligned}$$

This peculiar behavior near the backside of the streamer, at $\omega = -1$, shows up only in the rate of convergence.

Investigating the rate of convergence for $\tau \rightarrow \infty$, we first exclude a neighborhood of $\omega = -1$ and expand G in the integral (4.13) as

$$\begin{aligned} G\left(\frac{\rho\omega + T}{1 + \rho\omega T}\right) &= G(T) + (1 - T^2) \frac{\rho\omega}{1 + \rho\omega T} G'(T) + \mathcal{O}(1 - T^2)^2, \\ \text{where } G'(\omega) &= \partial_\omega G(\omega). \end{aligned}$$

With

$$1 - T^2 = 4e^{-\tau} + \mathcal{O}(e^{-2\tau}),$$

the integral yields

$$(4.15) \quad \frac{\tilde{\beta}(\omega, \tau)}{G'(1)} = \frac{4}{\omega^2} \left[\ln(1 + \omega) - \omega + \frac{\omega^2}{2} \right] e^{-\tau} + \mathcal{O}(e^{-2\tau}),$$

valid for

$$|1 + \omega| \gg |\omega|e^{-\tau}.$$

Thus outside the immediate neighborhood of $\omega = -1$, the shape for all smooth initial conditions with $G'(1) \neq 0$ converges exponentially in time as $e^{-\tau}$ along a universal path in function space, given in Eq. (4.15). For $G'(1) = 0$ the first non-vanishing term in the expansion of G dominates the convergence.

To analyze the neighbourhood of $\omega = -1$ we take the limit $\tau \rightarrow \infty$, with

$$(4.16) \quad s = (1 + \omega)e^\tau$$

fixed. We find

$$\begin{aligned} \frac{\tilde{\beta}(\omega, \tau)}{G'(1)} &= 4(\ln(2 + s) - \tau) e^{-\tau} \\ &+ \left\{ 2G'(1) + 4 \ln\left(\frac{2 + s}{4}\right) \left(G'\left(\frac{s - 2}{s + 2}\right) - G'(1) \right) \right. \\ &\quad \left. + (2 + s) \left(G(1) - G\left(\frac{s - 2}{s + 2}\right) \right) - 4 \int_0^{4/(2+s)} dy \ln y G''(1 - y) \right\} \frac{e^{-\tau}}{G'(1)} \\ (4.17) \quad &+ \mathcal{O}(\tau e^{-2\tau}). \end{aligned}$$

In terms of ω , the first contribution on the r.h.s. takes the form

$$4(\ln(2+s) - \tau) e^{-\tau} = 4e^{-\tau} \ln(2e^{-\tau} + 1 + \omega),$$

which shows that a logarithmic cut of $\tilde{\beta}(\omega, \tau)$ reaches $\omega = -1$ for $\tau \rightarrow \infty$, but with a prefactor vanishing exponentially in that limit. We thus have found a weak anomaly of the asymptotic relaxation near $\omega = -1$: In a spatial neighborhood of order $e^{-\tau}$ the exponential relaxation is modified by a factor τ . Furthermore, as mentioned above, all the initial structure of $\beta(\omega, 0)$ is compressed into that region. This is obvious from the occurrence of $G\left(\frac{s-2}{s+2}\right)$ etc., in Eq. (4.17).

To summarize, we have found that the shape of the interface for $\tau \rightarrow \infty$ converges to the circle along a universal slow manifold (4.15), except for a weak anomaly (4.17) at the backside at $\omega = -1$.

4.5. (Non-)analyticity of temporal eigenfunctions. In many cases, a full dynamical solution for arbitrary initial values cannot be found, and rather temporal eigenfunctions are searched for. However, in the present problem, functions $\beta(\omega, \tau)$ resulting from smooth initial conditions cannot exhibit exponential behavior in time for all τ , $0 \leq \tau < \infty$. This is seen easily by introducing

$$(4.18) \quad G(x) = \hat{G}\left(\frac{x-1}{x+1}\right),$$

writing $G(\zeta)$ in the equivalent form

$$(4.19) \quad G\left(\frac{\omega+T}{1+\omega T}\right) = \hat{G}\left(\frac{\omega-1}{\omega+1} e^{-\tau}\right),$$

and substituting this form into Eq. (4.4). Postulating strict exponential time behavior $\beta \sim e^{-\lambda\tau}$ one finds

$$(4.20) \quad \beta(\omega, \tau) \propto e^{\lambda\tau} \beta_\lambda(\omega), \quad \beta_\lambda(\omega) = \int_0^1 d\rho \rho \left(\frac{\omega\rho-1}{\omega\rho+1}\right)^\lambda.$$

Any eigenfunction $\beta_\lambda(\omega, 0)$ with $\lambda \neq 0$ clearly is singular either at $\omega = +1$, or at $\omega = -1$, or at both points. It therefore conflicts with smooth initial conditions. On the other hand, omitting a neighbourhood of $\omega = -1$, eigenfunctions exist for all $-\lambda \in \mathbf{N}_0$.

4.6. Completeness of the eigenfunctions near $\omega = 1$. In some neighborhood of $\omega = 1$, we even can show that any regular solution $\beta(\omega, \tau)$ can be expanded in terms of the ‘eigenfunctions’ $\beta_{-n}(\omega)$, $n \in \mathbf{N}_0$. This results from the Taylor expansion

$$(4.21) \quad \hat{G}(y) = \sum_{n=0}^{\infty} \hat{g}_n y^n,$$

which by assumption converges in a disk of radius $\hat{r} > 0$: Rewriting Eq. (4.4) as

$$(4.22) \quad \begin{aligned} \beta(\omega, \tau) &= \int_0^1 \frac{x dx}{\omega^2} G\left(\frac{x+T}{1+xT}\right) - \int_\omega^1 \frac{x dx}{\omega^2} G\left(\frac{x+T}{1+xT}\right) \\ &= \frac{M(T)}{\omega^2} - \sum_{n=0}^{\infty} \hat{g}_n e^{-n\tau} \int_\omega^1 \frac{x dx}{\omega^2} \left(\frac{1-x}{1+x}\right)^n \end{aligned}$$

and $\beta_{-n}(\omega)$ in a similar form as

$$(4.23) \quad \beta_{-n}(\omega) = \frac{M_n}{\omega^2} - \int_{\omega}^1 \frac{x dx}{\omega^2} \left(\frac{1-x}{1+x} \right)^n,$$

we find

$$(4.24) \quad \beta(\omega, \tau) = \frac{M(T)}{\omega^2} + \sum_{n=0}^{\infty} \hat{g}_n \left[\beta_{-n}(\omega) - \frac{M_n}{\omega^2} \right] e^{-n\tau}.$$

Provided $e^{-\tau} < \hat{r}$, we can separate the sum into the contribution $\propto 1/\omega^2$ and the rest. Since both $\beta(\omega, \tau)$ and the $\beta_{-n}(\omega)$ are regular at $\omega = 0$, the contributions $\propto 1/\omega^2$ have to cancel, which yields the final result

$$(4.25) \quad \beta(\omega, \tau) = \sum_{n=0}^{\infty} \hat{g}_n \beta_{-n}(\omega) e^{-n\tau}.$$

This result is valid for $e^{-\tau} < \hat{r}$ in the disk

$$\left| \frac{1-\omega}{1+\omega} \right| e^{-\tau} < \hat{r}.$$

It generalizes the asymptotic result (4.15) and shows that the $\beta_{-n}(\omega)$ in some sense form a complete set.

Indeed, the universal shape relaxation found in (4.15) together with the center of mass relaxation (4.11) precisely follow the slowest eigenfunction from (4.21) with $\lambda = -n = -1$.

4.7. Intermediate temporal growth and coupling of Fourier modes.

Having found that the space of regular functions does not allow for strictly exponential time behavior, we now consider the typical time variation of smooth perturbations. Before the exponential relaxation sets in, such perturbations typically will grow, and this growth can be quite dramatic. As an illustration we consider a perturbation defined by

$$G(\omega) = \omega^k, \quad k \gg 1,$$

corresponding to initial conditions

$$(4.26) \quad \beta(\omega, 0) = \frac{\omega^k}{k+2}.$$

For $T = 1 - e^{-\theta}/k$, corresponding to times $\tau = \theta + \ln(2k) + \mathcal{O}(1/k)$, we can write

$$G\left(\frac{\omega+T}{1+\omega T}\right) = \left(\frac{1 - \frac{e^{-\theta}}{1+\omega} \frac{1}{k}}{1 - \frac{\omega e^{-\theta}}{1+\omega} \frac{1}{k}}\right)^k = \exp\left[-e^{-\theta} \frac{1-\omega}{1+\omega}\right] \left(1 + \mathcal{O}\left(\frac{1}{k}\right)\right),$$

where we again excluded some neighborhood of $\omega = -1$. Substituting this expression into Eq. (4.13) we find on the unit circle $\omega = e^{i\alpha}$:

$$(4.27) \quad \begin{aligned} & \tilde{\beta}(e^{i\alpha}, \tau) \\ &= \int_0^1 d\rho \rho \exp\left[-e^{-\theta} \frac{1-\rho^2 - 2i\rho \sin \alpha}{1+\rho^2 + 2\rho \cos \alpha}\right] - \frac{1}{2} \exp[-e^{-\theta}] + \mathcal{O}\left(\frac{1}{k}\right). \end{aligned}$$

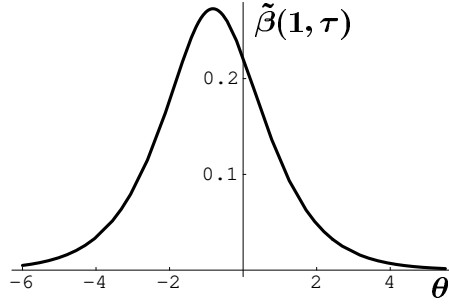


FIG. 4.1. $\tilde{\beta}(e^{i\alpha}, \tau)$ from Eq. (4.27) for $\alpha = 0$ as a function of subtracted time $\theta = \tau - \ln 2k$.

Figure 4.1 shows this function, evaluated at $\alpha = 0$ ($\omega = 1$). The behavior is quite peculiar. Up to times of order $\ln k$ the perturbation stays of order $1/k \ll 1$, then it increases roughly exponentially up to values of order 1, and finally it decreases again exponentially, approaching the slow manifold (4.15). Thus for very large k the initial perturbation $\beta(\omega, 0) \sim 1/k$ in some time interval can be amplified by a factor of order k , and Eq. (4.27) shows that the leading behavior in that time interval is independent of k .

Closer analysis shows that in terms of a formal Fourier expansion

$$(4.28) \quad \tilde{\beta}(e^{i\alpha}, \tau) = \sum_{n=1}^{\infty} a_n(\tau) e^{in\alpha},$$

the amplification is carried by the low modes, $n = \mathcal{O}(1)$. As will be illustrated by an explicit example below, cf. figure 5.2b, in such a mode representation the time evolution feeds the strength of the perturbation successively into lower and lower modes. This is equivalent to the observation that the automorphism $e^{i\alpha} \rightarrow \zeta(e^{i\alpha}, T)$ drives all the perturbative structure towards $\alpha = \pi$ and smoothens the remainder of the interface. Note, however, that starting with a perturbation $\sim \omega^k$ in the course of time also modes $n > k$ are (weakly) populated to build up a complicated structure near $\omega = -1$. We recall that for the unregularized model $\epsilon = 0$, the time evolution of a perturbation $\propto \omega^k$ populates only modes $k \leq n$ [4].

4.8. Motion of the zeros of $\partial_\omega f$ and cusps. So far we have shown that the propagating circle is linearly stable, i.e., we implicitly considered perturbations of infinitesimal strength η . The full nonlinear evolution of a finite perturbation is beyond the scope of this paper. Still, it clearly is a question of practical interest, whether a finite perturbation evolving under the linearized dynamics, for all times satisfies the assumptions underlying the conformal mapping approach. For the mapping to stay conformal, all the zeros of $\partial_\omega f(\omega, \tau)$ must stay outside the unit circle. We thus here analyze the roots of the equation

$$(4.29) \quad 0 = \partial_\omega f(\omega, \tau) = -\frac{1}{\omega^2} + \eta \partial_\omega \beta(\omega, \tau).$$

Using Eqs. (4.3), (4.4), we can rewrite this equation as

$$(4.30) \quad 2\eta \int_0^1 d\rho \rho \left[G\left(\frac{\omega + T}{1 + \omega T}\right) - G\left(\frac{\rho\omega + T}{1 + \rho\omega T}\right) \right] = \frac{1}{\omega}.$$

With our normalization (4.7) of G , for all ω in the closed unit disk the l.h.s. of this equation is bounded by $2|\eta|$. We conclude that the bound

$$(4.31) \quad |\eta| < \frac{1}{2}$$

guarantees that within the framework of first order perturbation theory the mapping stays conformal for all times. To get some feeling for this estimate we note that for $G(\omega) = \omega^k$ the map initially (for $\tau = 0$) is conformal provided $|\eta| < 1 + 2/k$. Thus the bound (4.31) is quite strong. We now will show that in general it cannot be improved.

For $\tau \rightarrow \infty$, zeros of $\partial_\omega f(\omega, \tau)$ reach $\omega = -1$, which is a consequence of the fact that in this limit an infinitesimally small neighborhood of $\omega = -1$ under the mapping $\omega \rightarrow \zeta$ is mapped essentially on the whole complex plane. We now analyze this limit for the simple example $G(\omega) = \omega$. Substituting this form into the asymptotic behavior (4.17) and using the definition (4.16) of s , we find

$$\partial_\omega \beta = \frac{4}{2+s} + \mathcal{O}(\tau e^{-\tau}).$$

Eq. (4.29) reduces to $s = 4\eta - 2$, showing that a zero ω_0 of $\partial_\omega f(\omega, \tau)$ approaches $\omega = -1$ as

$$\omega_0 = -1 + (4\eta - 2)e^{-\tau}.$$

For ω_0 to come from outside the unit circle we clearly must have

$$(4.32) \quad \Re[\eta] < \frac{1}{2}.$$

In all the discussion of this section we have assumed the initial boundary to be smooth, so that all derivatives $\partial_\omega^n G(\omega)$ exist on the boundary $|\omega| = 1$. Inspecting the results it is obvious that this assumption can be considerably relaxed, since only those derivatives which show up explicitly, have to exist. Thus, for exponential relaxation (4.15) outside the neighborhood of $\omega = -1$ to prevail, the existence of $\partial_\omega G(\omega)$ is sufficient, which amounts to the condition that the curvature of the initial boundary is well defined. For the circle to be linearly stable, Eq. (4.14), it is sufficient that $G(e^{i\alpha})$ is bounded and continuous, which implies that the boundary has a well defined slope.

If the initial boundary shows a cusp, the time evolution sensitively depends on the details. If the cusp is found in forward direction, so that $G(\omega)$ diverges for $\omega \rightarrow 1$, the streamer will be strongly accelerated. In a related model [12], such an effect has been pointed out before. Furthermore the shape will not relax to a circle, and the conformal map will presumably break down at finite time. If the cusp does not affect the analyticity of $G(\omega)$ near $\omega = 1$, it is convected towards the back and broadened, whereas the front of the streamer approaches the circular shape. Still, however, conformality of the map may break down at finite time.

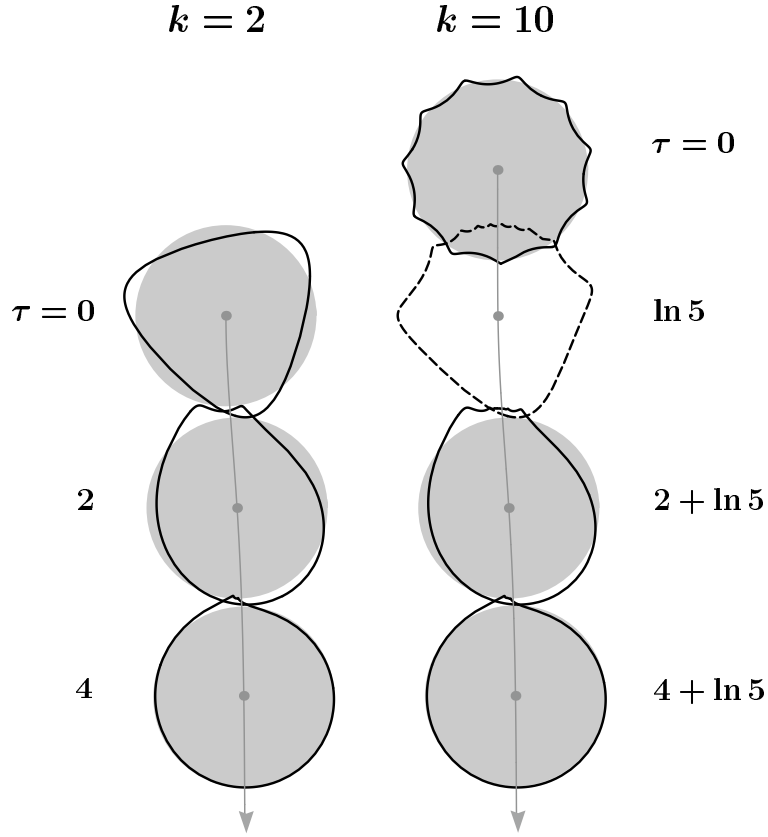


FIG. 5.1. Snapshots of the evolution of the streamer for $k = 2$ (left column) and $k = 10$ (right column) at the indicated instants of time. The solid lines represent the perturbed interfaces. The gray disks move with the center of mass velocity (5.4) of the perturbed circles. One gray disk has been omitted for clarity. See the text for further discussion.

5. Explicit examples for $\epsilon = 1$. We here illustrate the general results by some examples.

5.1. The evolution of Fourier perturbations. We first consider perturbations of the form

$$(5.1) \quad \beta^{[k]}(\omega, 0) = \frac{\omega^k}{k+2}, \quad \text{i.e. } G(\omega) = \omega^k.$$

The integral (4.4) is easily evaluated to yield

$$(5.2) \quad \beta^{[k]}(\omega, \tau) = \frac{1}{2\omega^2 T^2} \left\{ T^k + ((T\omega)^2 - 1) \zeta^k + k(1 - T^2) \left[T^k - (\omega T + 1) \zeta^k + \frac{1 + k + T^2(1 - k)}{T^k} \cdot \left(\ln(1 + \omega T) - \sum_{\nu=1}^{k-1} \frac{T^\nu}{\nu} (\zeta^\nu - T^\nu) \right) \right] \right\},$$

where $T = T(\tau)$ and $\zeta = \zeta(\omega, T(\tau))$ are given by Eqs. (3.9), or (3.10), respectively. In figure 5.1 we have plotted snapshots of the resulting motion of the interface, determined as

$$(5.3) \quad z = x + iy = \frac{1}{\omega} + \tau + \eta \beta^{[k]}(\omega, \tau), \quad \omega = e^{i\alpha}, \quad 0 \leq \alpha \leq 2\pi.$$

The direction of motion, i.e. the positive x -direction, is downwards. Together with the moving interface we show the unperturbed circular streamer at different times as gray disks with the center moving according to

$$(5.4) \quad z_{\text{cm}}(\tau) = \tau + \frac{\eta}{2} G(T(\tau)) = \tau + \frac{\eta}{2} \tanh^k \frac{\tau}{2},$$

as predicted for the center of mass motion for the perturbed streamer in Eq. (4.10).

In figure 5.1 we perturbed the circle by $\eta \beta^{[k]}$, $k = 2$ or $k = 10$, using the same parameter $\eta = 0.6e^{i\pi/4}$ in both cases. The starting position for $k = 10$ is shifted relative to that for $k = 2$ by a distance corresponding to $\Delta\tau = \ln 5$. As discussed below Eq. (4.27), for $1 \ll k_1 < k_2$ we expect

$$\beta^{[k_1]}(\omega, \tau) \approx \beta^{[k_2]}(\omega, \tau + \ln(k_2/k_1)).$$

Figure 5.1 illustrates that such a ‘universality’ for the gross structure holds down to very small k . (Of course the choice of differing values of η would distort the figures and mask this feature.) Basically during time evolution the initial maximum closest to the forward direction is smeared out and builds up the asymptotic circle, whereas all other structures are compressed at the backside. For $k = 10$ the complicated structure at the back is magnified in figure 5.2a. Figure 5.2b shows the time dependence of the coefficients a_n of the low modes $e^{in\alpha}$ in the expansion (4.28), again for $k = 10$. It illustrates how the strength of the perturbation cascades downwards in n and increases in time, until it completely is absorbed into the lowest mode, i.e., the overall shift of the circle. We should recall, however, that also modes $n > k$ are weakly populated to build up the structure at the back.

For $k = 2$, figure 5.3 shows the motion of the zeros of $\partial_\omega f(\omega, \tau)$ in the complex ω -plane, as discussed in section 4.8. It corresponds to the $k = 2$ part of figure 5.1. Two zeros, which initially are close to the backside of the unit circle, for $\tau \rightarrow \infty$ approach $\omega = -1$. They clearly are associated with the two maxima that in the comoving frame are convected towards $z = x + iy = -1$. The third zero, originally found close to $\omega = +1$, after a large excursion leaves the physical sheet at time $\tau \simeq 2.51$. The logarithmic cut is on the negative axes, with the branchpoint $\omega_{\text{bp}} = -1/T(\tau)$ reaching $\omega = -1$ for $\tau \rightarrow \infty$.

5.2. The evolution of localized perturbations. We finally consider some more localized perturbation, defined by

$$(5.5) \quad G(\omega) = \frac{(1-\gamma)e^{i\alpha_0}}{\omega - \gamma e^{i\alpha_0}}, \quad \gamma > 1,$$

corresponding to an initial perturbation

$$(5.6) \quad \eta \beta(\omega, 0) = \eta \frac{(1-\gamma)\gamma}{\omega^2} e^{2i\alpha_0} \left[\ln \left(1 - \frac{\omega}{\gamma} e^{-i\alpha_0} \right) - \frac{\omega}{\gamma} e^{-i\alpha_0} \right].$$

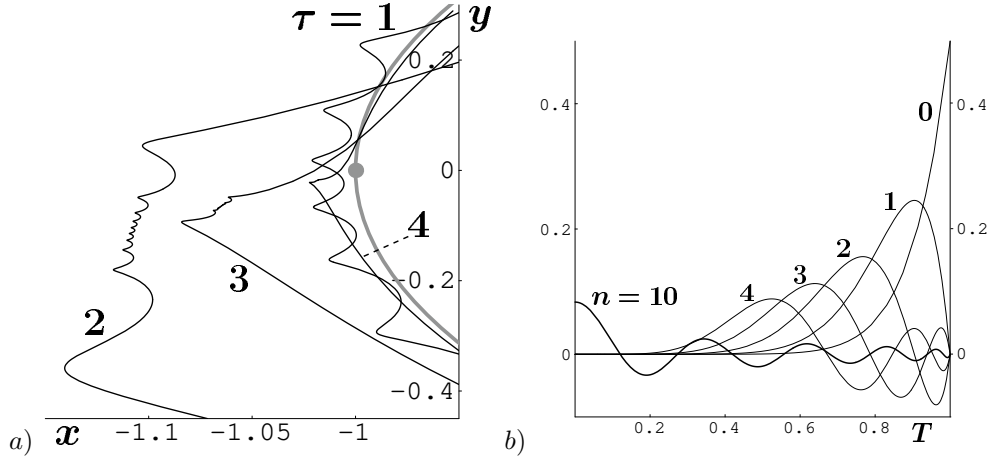


FIG. 5.2. a) Magnified plot of the backside of the streamer for $k = 10$, $\eta = 0.6 e^{i\pi/4}$ (as in the right column of figure 5.1) for the τ values given. The overall motion is subtracted. We observe the compression of the fine structure and the intermediate growth of the perturbation. Asymptotically for $\tau \rightarrow \infty$, the structure converges to the gray circle. In the comoving frame, the gray dot marks $x + iy = -1$ which is the point to which the structure finally is contracted. Note that the scale of x is stretched compared to that of y , and that the figure is turned relative to figure 5.1. b) The amplitudes a_n as in Eq. (4.28) as a function of T for $k = 10$; the values of n are given.

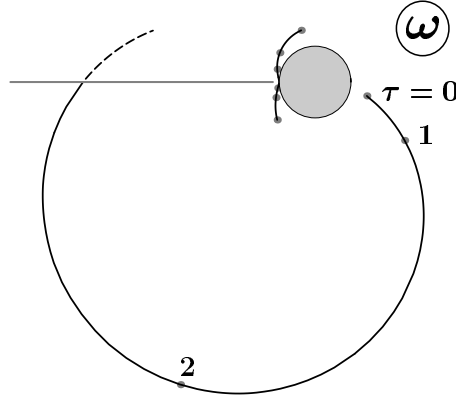


FIG. 5.3. Motion of the zeros of $\partial_\omega f$ in the ω -plane for $k = 2$ and $\eta = 0.6 e^{i\pi/4}$ (as in the left column of figure 5.1). The dots give the position for $\tau = 0, 1, 2$. The horizontal line is the cut for $\tau = 2.51$, where one zero enters the second sheet (broken curve). The unit disk is also shown.

The result for $\beta(\omega, \tau)$ reads

$$(5.7) \quad \beta(\omega, \tau) = \frac{(\gamma - 1)e^{i\alpha_0}}{\gamma e^{-i\alpha_0} - T(\tau)} \left\{ \frac{T(\tau)}{2b(\tau)} - \left(1 - \frac{T(\tau)}{b(\tau)}\right) \frac{\ln(1 + b(\tau)\omega) - b(\tau)\omega}{(b(\tau)\omega)^2} \right\},$$

where

$$(5.8) \quad b(\tau) = \frac{1 - T(\tau)\gamma e^{i\alpha_0}}{T(\tau) - \gamma e^{i\alpha_0}}.$$

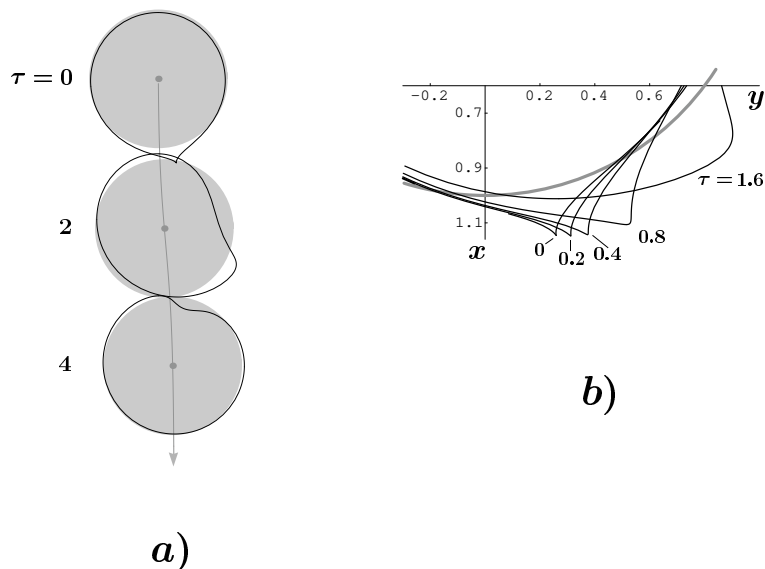


FIG. 5.4. *a) Time evolution of a localized perturbation as described in the text. b) Evolution of the initial peak for shorter times as indicated. The overall motion of the streamer is subtracted. A part of the asymptotic circle is shown in gray.*

We note that $b(\tau) \rightarrow 1$ for $T(\tau) \rightarrow 1$, so that in the large time limit the logarithmic cut reaches $\omega = -1$. As discussed in the context of Eq. (4.17), this is a generic feature of the present problem. Our choice of parameters $\gamma = 1.1$, $\alpha_0 = -\pi/12$, $\eta = 1.5$, almost produces a cusp in the initial condition: the only zero of $\partial_\omega f(\omega, 0)$ is found at $\omega_0 = 1.001 \exp(-.243i)$. This zero, however, is driven away from the unit circle and leaves the physical sheet. Another zero that entered the physical sheet somewhat earlier, for $\tau \rightarrow \infty$ reaches $\omega = -1$. Figure 5.4a shows snapshots of the time evolution of the perturbed interface in a representation like figure 5.1. It illustrates how the peak rapidly is smeared out and the interface becomes smooth. Figure 5.4b follows the evolution of the peak for short times and shows how it is convected and broadened.

We should note that in the special case, where the initial peak strictly points in forward direction ($\alpha_0 = 0$), convection cannot take place. The peak simply is broadened and vanishes, whereas some new peak shows up at the back for intermediate times.

6. Conclusions. As already summarized in the introduction, we here have shown that a circle, moving according to the gradient of a Laplacian field and driven by an external field that becomes constant far from the circle, is stabilized by a sufficiently strong boundary condition of kinetic undercooling type. Our explicit rigorous time dependent solution, valid for arbitrary smooth initial conditions and a special value of a parameter specifying the boundary condition, shows that a convective mechanism plays an important role in the stabilization. Perturbations of the circle are convected to the back, where they decay in some quite nontrivial fashion. Mathematically, convection is embodied in the automorphisms of the unit disk with fixed points ± 1 . These automorphisms dominate the dynamical behavior in both rigorously solvable nontrivial cases $\epsilon = 1$ and $\epsilon = \infty$. Also in the general case, where we cannot solve the PDE resulting from linear stability analysis analytically, these automorphisms are

intimately connected to the structure of the problem. We therefore expect convective stabilization to occur quite generally in the regularized problem. Work in this direction is in progress.

Concerning the significance of our results in a physical context we note that the dynamics at the backside of the propagating circles, which is mathematically quite interesting, is of no relevance for real discharges. However, it may be relevant for other physical phenomena like electromigration, which lead to mathematically similar models. The dynamics of the front part of the physical streamer can be expected to be adequately captured by our model. We therefore expect convective stabilization to play an important role in physical discharges.

We acknowledge helpful and motivating discussions with F. Brau, A. Doelman, J. Hulshof, H. Levine, L.P. Kadanoff, S. Tanveer and S. Thomaë.

Appendix A. The limit $\epsilon \rightarrow \infty$.

For $\epsilon \rightarrow \infty$, the PDE (3.7) with the form (3.11) of \mathcal{L}_ϵ reduces to

$$(A.1) \quad \left(h(\zeta, T) \partial_\zeta + 1 \right) \partial_T \hat{\beta}(\zeta, T) = 0, \quad \text{where } \hat{\beta}(\zeta, T) \equiv \beta(\omega, \tau).$$

Eq. (A.1) allows for a large set of solutions obeying the same initial condition

$$(A.2) \quad \beta(\omega, 0) = \beta_0(\omega),$$

but imposing regularity on the unit disk \mathcal{U}_ω , we single out the simple form

$$(A.3) \quad \beta(\omega, \tau) = \beta_0(\zeta).$$

Thus for $\epsilon = \infty$, the dynamics is simply given by the automorphisms $\omega \rightarrow \zeta(\omega, T)$. This implies that $\beta(\omega, \tau)$ is bounded uniformly in τ as

$$(A.4) \quad |\beta(\omega, \tau)| \leq \max_{\omega \in \partial \mathcal{U}_\omega} |\beta_0(\omega)|,$$

so that in contrast to the case $\epsilon = 1$, there is no intermediate growth of the perturbations.

The shift of the center of mass is given by (cf. Eq. (4.10)):

$$(A.5) \quad \beta(0, \tau) = \beta_0(T(\tau)) = \beta_0(1) - 2 \beta'_0(1) e^{-\tau} + \mathcal{O}(e^{-2\tau}),$$

and except for the point $\omega = -1$, the shape again converges exponentially in time to the circle along the universal slow manifold

$$(A.6) \quad \beta(\omega, \tau) - \beta(0, \tau) = \beta'_0(1) \frac{4\omega}{1+\omega} e^{-\tau} + \mathcal{O}(e^{-2\tau}),$$

cf. Eq. (4.15) for $\epsilon = 1$. Again the neighbourhood of $\omega = 1$ for time $\tau = 0$, more precisely $\beta_0(1)$ and $\beta'_0(1)$, determine the long time convergence. Since by assumption $\beta_0(\omega)$ is analytical at $\omega = 1$, evidently an eigenfunction expansion in the sense of subsection 4.5 exists.

The only major difference to the case $\epsilon = 1$ concerns the point $\omega = -1$. Clearly,

$$(A.7) \quad \beta(-1, \tau) \equiv \beta_0(-1)$$

independently of τ , and indeed for $\tau \rightarrow \infty$ the conformality of the mapping breaks down in the neighbourhood of $\omega = -1$ since $\partial_\omega \beta(\omega, \tau)|_{\omega=-1}$ diverges.

REFERENCES

- [1] U. EBERT, W. VAN SAARLOOS AND C. CAROLI, *Streamer propagation as a pattern formation problem: planar fronts*, Phys. Rev. Lett. **77** (1997) 4178.
- [2] M. ARRAYÁS, U. EBERT AND W. HUNSDORFER, *Spontaneous branching of anode-directed streamers between planar electrodes*, Phys. Rev. Lett. **88** (2002) 174502.
- [3] M. ARRAYÁS AND U. EBERT, *Stability of negative ionization fronts: regularization by electric screening?*, Phys. Rev. E **69** (2004) 056220.
- [4] B. MEULENBROEK, A. ROCCO, U. EBERT, *Streamer branching rationalized by conformal mapping techniques*, Phys. Rev. E **69** (2004) 067402.
- [5] U. EBERT, C. MONTIJN, T.M.P. BRIELS, W. HUNSDORFER, B. MEULENBROEK, A. ROCCO, E.M. VAN VELDHUIZEN, *The multiscale nature of streamers*, Plasma Sources Sci. Techn. **15** (2006) S118.
- [6] D. BENSIMON, L.P. KADANOFF, S. LIANG, B.I. SHRAIMAN, C. TANG, *Viscous flows in two dimensions*, Rev. Mod. Phys. **58** (1986) 977.
- [7] L.I. RUBINSTEIN, *The Stefan problem*, Translations of Mathematical Monographs **27** (AMS, Providence 1971).
- [8] P.S. HO, *Motion of inclusion induced by a direct current and a temperature gradient*, J. Appl. Phys. **41** (1970) 64.
- [9] M. MAHADEVAN, R.M. BRADLEY, *Stability of a circular void in a passivated, current-carrying metal film*, J. Appl. Phys. **79** (1996) 6840.
- [10] G. TAYLOR, P.G. SAFFMAN, *A note on the motion of bubbles in a Hele-Shaw cell and porous medium*, Quart. J. Mech. and Appl. Math. **XII**, Pt. 3 (1959) 255.
- [11] S. TANVEER, P.G. SAFFMAN, *Stability of bubbles in a Hele-Shaw cell*, Phys. Fluids **30** (1987) 2624.
- [12] D.C. HONG, F. FAMILY, *Bubbles in the Hele-Shaw cell: Pattern selection and tip perturbations*, Phys. Rev. A **38** (1988) 5253.
- [13] V.M. ENTOV, P.I. ETINGOF, D.YA. KLEINBOCK, *Hele-Shaw flows with a free boundary produced by multipoles*, Eur. J. Appl. Math. **4** (1993) 97.
- [14] B. MEULENBROEK, U. EBERT, L. SCHÄFER, *Regularization of moving boundaries in a Laplacian field by a mixed Dirichlet-Neumann boundary condition: exact results*, Phys. Rev. Lett. **95** (2005) 195004.
- [15] S.D. HOWISON, *Complex variable methods in Hele-Shaw moving boundary problems*, Eur. J. Appl. Math. **3** (1992) 209.
- [16] F. BRAU, U. EBERT, B. MEULENBROEK, L. SCHÄFER, *Local dynamics on curved moving boundaries with kinetic undercooling*, in preparation for Phys. Rev. E
- [17] YU.E. HOHLOV, M. REISSIG, *On classical solvability for Hele-Shaw moving boundary problems with kinetic undercooling regularization*, Eur. J. Appl. Math. **6** (1995) 421.
- [18] M. REISSIG, S.V. ROGOSIN, F. HÜBNER, *Analytical and numerical treatment of a complex model for Hele-Shaw moving boundary value problems with kinetic undercooling regularization*, Eur. J. Appl. Math. **10** (1999) 561.
- [19] S.J. CHAPMAN, J.R. KING, *The selection of Saffman-Taylor fingers by kinetic undercooling*, J. Engineering Math. **46** (2003) 1.
- [20] S. RICHARDSON, *Hele Shaw flows with a free boundary produced by the injection of fluid into a narrow channel*, J. Fluid Mech. **56** (1972) 609.